PROSPECTS FOR ENHANCED SINGLE-WELL HEAT EXTRACTION

Peter Leary[1], Justin Pogacnik[1], and Peter Malin[1]

[1]Institute of Earth Science & Engineering, University of Auckland, 58 Symonds Street, Auckland 1142, New Zealand

p.leary@auckland.ac.nz

Keywords: *Geothermal energy, permeability enhancement, thermal advection, heat pump performance*

ABSTRACT

Higher temperature fluid from a single well viewed as a thermal-conduction-bound heat pump may be possible by enhancing near-wellbore permeability to allow a greater effective wellbore radius. Heat advection simulation in 2D estimates the degree to which increased permeability about a wellbore can be expected to increase single well heat productivity. We find that for representative circumstances, heat extraction via wellbore-vicinity advective flow could increase recovered fluid temperature to ~200°C from ~100°C available via a thermal conduction-based heat pump. Prospects for higher heat extraction through enhanced *in situ* flow in the vicinity of a wellbore − possibly through thermal shock but also through *in situ* fluid pressurisation − could underwrite scientific and/or engineering investigations directed to larger questions posed by EGS.

1. INTRODUCTION

The heat-pump principle of single-well heat extraction by circulating wellbore fluids is usually confined to thermal conduction between juxtaposed fluid and solid (e.g., Ramey 1962; Kwon 1998). We here consider the heat-pump principle of single-well heat extraction in more general terms in which heat-pump fluids can exit the wellbore into the surrounding medium then re-access the heat pump plumbing for ascent to the surface. Such flow systems, if realisable, can produce more heat per wellbore cost than is possible by conduction-limited heat exchange at wellbore radii.

In order to realise such a flow system, we have to envision a strategy by which a rockmass annular volume surrounding a wellbore is conditioned to allow flow within the annulus without undue loss at the annular radius. Standard hydrofracking of the wellbore radius would not, for instance, be considered a likely candidate for such annular flow stimulation; fluids exiting the wellbore along a hydrofracture aperture would simply disappear into the greater rockmass. Rather we have in mind a completely different approach to flow stimulation adjacent to a wellbore.

Our approach to *in situ* flow is based on a systematic inspection of crustal rock fluid flow distributions which shows that *in situ* flow can be considered, to first order, as spatially complex and erratic percolation along pre-existing fracture-connectivity pathways. We are supposing that such pre-existing pathways offer a means by which *in situ* fluids adjacent to the wellbore can be slowly pressurized to increase both the degree of fracture-connectivity and the capacity for the fracture-connectivity pathways to conduct fluids. In short, our approach to *in situ* flow stimulation is explicitly to duplicate, and accelerate, the natural processes by which the complex and erratic *in situ* flow structures are created in the first place.

Our concept of *in situ* flow stands in considerable contrast to the standard view of seepage through an essentially uniform porous medium. Uniform seepage flow suggests little systematic means by which flow stimulation can be achieved outside the hydrofracture process. Our view of *in situ* flow as fluid percolation along spatially erratic fracture-defect pathways everywhere present *in situ* focuses on *in situ* heterogeneity as a given (Leary, Pogacnik & Malin 2012a-c; Leary et al 2013a-c; Pogacnik, Leary & Malin 2012, 2013). We seek to exploit that heterogeneity to increase the effective annular radius of fluid flow through engineered fluid pressurisation processes that build on natural fluid-rock coupling processes. We see below that flow at larger *in situ* flow radii enables the fluid to pick up heat at higher temperatures than does flow confined to the smaller wellbore radii.

We first discuss how the fluid temperature of a wellbore heat conduction system depends on wellbore radius, hence why it is worth seeking a larger 'effective wellbore radius' to boost the temperature of the wellbore fluid as could in principle be achieve by fracture-stimulating rock near the inner radius. We then use 2D numerical simulations of advective flow from an outer radius to an inner radius to estimate the contrast between advective and conductive heat transfer from country rock to a wellbore. The computations suggest an effective range of advective wellbore radii larger than that feasible with wellbores operating on thermal conductivity principles. In order to give a more explicit view of the *in situ* heterogeneity nature of fluid flow on which we base our heat transfer discussion, we note in an appendix a numerical realisation of the means by which the effective radius of a single wellbore might be increased to allow heat extraction via advective flow at suitably large effective wellbore radii. We do not, however, seek to cover important engineering issues by which such a wellbore-annular flow system can be effectively plumbed.

2. HEAT EXTRACTION FLUID TEMPERATURE IN RELATION TO WELLBORE RADII (THERMAL CONDUCTIVITY TRANSPORT = HEAT PUMP)

Steady state and heat-diffusion time-evolving flow in a cylindrical annular geometry within a uniform medium (no azimuthal variation and no axial flow) are formulated in Chapter 7 of Carslaw and Jaeger (1959). The steady state radial heat flow equation for flow in a section normal to the cylinder axis, $\partial(r\partial T/\partial r)/\partial r = 0$, has logarithmic solution form for temperature T, $T(r) = a\ log(r) + b$. The time-evolving cylindrical radial heat flow equation $1/r\partial(r\partial T/\partial r)/\partial r = 1/D\ \partial T/\partial t$ has solution forms comprising Bessel functions weighed by exponential time-terms like $exp(-\gamma^2 Dt)$, γ being associated with the zeros of the Bessel functions. The time scale for thermal flow reaching the steady-state for a given radial dimension is fixed by the thermal diffusivity of rock $D = K/\rho c \sim 2{\cdot}10^{-6}$ m^2/s given by highly representative values of thermal conductivity $K \sim 3$ W/m·°C, mass density $\rho \sim 2000$kg/m^3, and heat capacity $c \sim$ 840 J/kg·°C.

A commercial-scale single-well heat extraction facility may be approximated as producing QL watts of fluid–borne heat, for Q as average heat produced per unit wellbore length over wellbore production interval L. Setting QL = 1MW$_{th}$ for a km-long well interval L = 1000m, Q = 1kW/m.

Applying the steady-state radial heat flow equation $\partial(r\partial T/\partial r)/\partial r = 0$ solution form $T(r) = a\ log(r) + b$ to the case of a wellbore of radius r_1 extracting heat from a co-located cylindrical volume of radius $r_2 >> r_1$ with ambient boundary temperature T_2, the constant $a = -\ q_1 r_1/K$ for $K \sim 3$ W/m·^{o}C and $q_1 = Q/r_1$ W/m^2 at each meter interval of wellbore. The wellbore temperature for steady-state heat flow, $T_1 = T_2 - T_0\ log(r_2/r_1)$, is seen to decline logarithmically with decreasing wellbore radius, $T_0 log(r_2/r_1)$, for T_0 = Q/K ~ 1000W/m/3W/m·^{o}C ~ 333^{o}C. Comparing wellbore fluid extraction temperatures at radii r_1 0.1m and 1m for heat system radius r_2= 10m, the temperature difference is $T_0 log(0.1/1) = 333^oC/2.3 = 145^oC$.

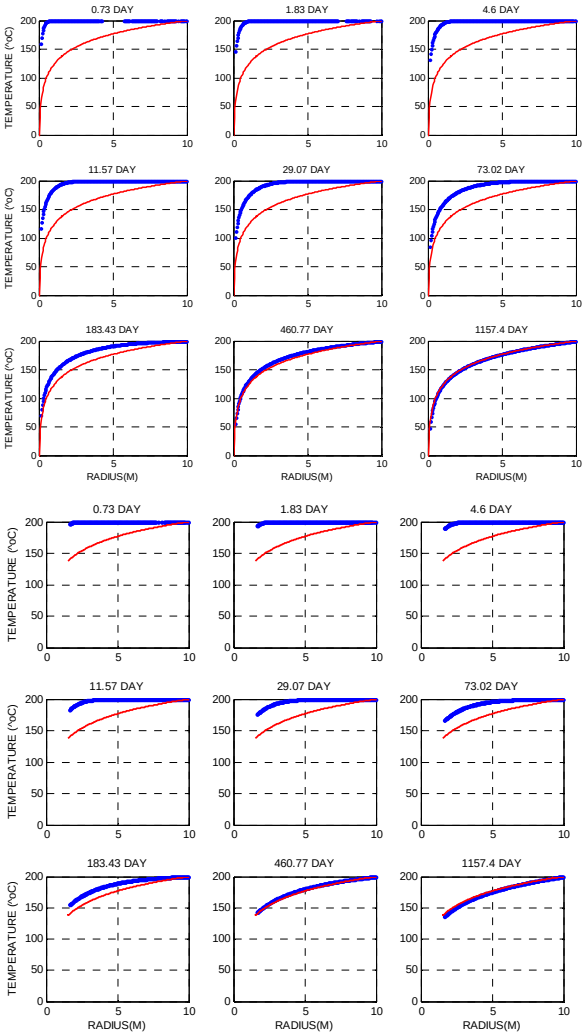

Figure 1: Plot-sets for annular heat flow systems of 10m radius; upper plot set = 10cm inner wellbore; lower plot set = 1m inner wellbore. Red lines denote analytic steady-state heat flow radial temperature profiles for each wellbore radius. Blue lines denote time evolving temperature radial profile computed by the Matlab PDE solver; the numerical blue line solutions agree with time-evolving analytic solutions.

Fig 1 illustrates the different radial temperature distributions in a section normal to the wellbore axis for wellbore radii 0.1m and 1m as red lines in each plot (upper plot set for 0.1m wellbore, lower plot set for 1m wellbore). The difference in wellbore steady state temperatures, seen in the lower-right plots of each plot set for the two wellbore radii, is ~145^{o}C. This result clearly favours heat extraction from a ~1m wellbore over heat extraction from a ~10cm wellbore, and sets the scene for our discussion of single well heat extraction from crustal rock taken as a geocritical poroperm medium.

The sequences of blue lines in the two Fig 1 plot-sets (0.1m/1m wellbore radii at upper/lower) show time-evolving temperature profiles from early times (plot set upper left) to steady-state (plot-set lower right). The time-evolution curves were computed using Matlab's 2D PDE finite-element solver for a cylindrical geometry of inner radii 0.1m and 1m and outer radius 10m. The effective equilibration time given by thermal diffusivity D is ~1yr for a system of dimension 10m. The time evolving analytic solution $T(r,t) = 2T_0/a\ \Sigma_k\ J_0(\gamma_k r)/\gamma_k J_1(\gamma_k a)\ exp(-D\gamma_k^2 t)$, $J_0(.)$ and $J_1(.)$ respectively Bessel functions of zero and first order, agrees with the Matlab PDE computed curves.

We see from Fig 1 that in purely thermal conduction terms, increasing the effective radius of a wellbore heat-extraction fluid flow system from ~10cm to ~150cm can raise wellbore extraction fluid temperatures from ~50^{o}C to ~150^{o}C. We now use the Matlab 2D PDE solver to consider a similar computational comparison for fluid advection systems for a range of assumed permeability enhancements in 3m and 10m radial annuli about the wellbore. The appendix details the empirical basis of our permeability enhancement procedure.

3. HEAT EXTRACTION VIA NEAR-WELLBORE ADVECTIVE HEAT TRANSPORT

Heat advection can be expressed in the Matlab PDE solver as a spatially variable advective heat source $Q(T) \equiv \rho_f c_f \nabla\cdot(\boldsymbol{v}T)$ transporting heat for a known fluid velocity field $\boldsymbol{v}(x,y)$ but unknown temperature field $T(x,y)$; the factor $\rho_f c_f$ accounts for fluid heat transport capacity. Steady state flow field $\boldsymbol{v}(x,y)$, fixed by a spatial distribution of constant pressure sources/sinks within a temporally constant but spatially variable permeability distribution $\kappa(x,y)$, gives temperature distribution $T(x,y)$,

$$-\nabla^2 T\,(x,y) = \varsigma[\nabla\cdot\boldsymbol{v}T\,(x,y) + \boldsymbol{v}\cdot\nabla T(x,y)]$$

$$= \varsigma[(v_{xx} + v_{yy})T + (v_x T_x + v_y T_y)], \qquad (1)$$

for $\varsigma = \rho_f c_f/K \sim 10^6$ s/m^2, fluid flow vector and gradient fields $v_x(x,y)$, $v_y(x,y)$, $v_{xx}(x,y)$ and $v_{yy}(x,y)$, and rock thermal conductivity $K \sim 3$W/m·^{o}C, fluid mass density $\rho \sim$ 1000kg/m^3 and fluid heat capacity $c \sim$ 4180J/kg·^{o}C.

Advective flow steady-state temperature distribution for a 16cm radius wellbore extracting heat at rate 4000W/m (four times the rate of Fig 1) is given in Fig 2 for a 300^{o}C ambient temperature fixed at a 10m annular radius. With low advective flow at high heat extraction rate, the produced wellbore fluid temperature is ~ 80^{o}C, essentially the temperature to which thermal conduction would constrain heat extraction (as, for instance, the Fig 1 heat flow simulations).

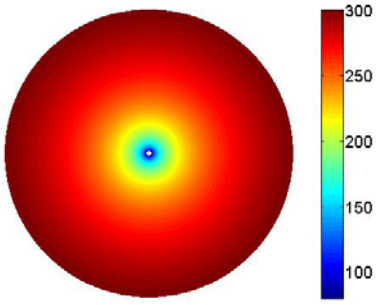

Figure 2: Radial temperature profile for 10m annular poroperm medium at 300°C ambient temperature centered on 16cm wellbore extracting heat at rate 4kW/m. For small advective flow from outer boundary to wellbore, the annular temperature profile is essentially determined by conduction, resulting in a wellbore heat extraction fluid temperature below 100°C.

The essentially thermal conductivity-constrained Fig 2 temperature distribution can be compared with distributions for higher rates of advective flow. Higher advective flow can be associated with progressive permeability distributions such as given in Fig 3 (see appendix for details). The higher permeabilities of Fig 3 give temperature distributions in Figs 4-6, producing wellbore flow temperatures of ~120°C, ~180°C and ~210°C in contrast with the thermal conduction limit of order ~80°C.

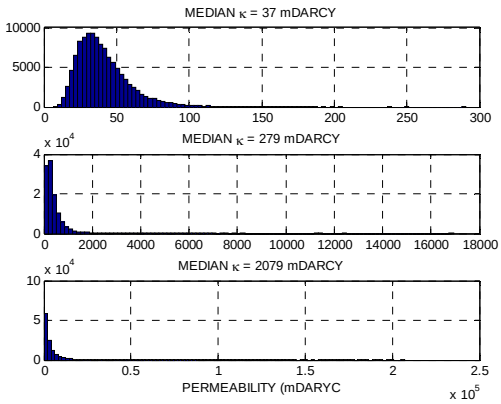

Figure 3: Representative permeability population distributions for the permeability enhancement sequence for Figs 4-6 (see appendix for details). The permeability sequence begins with distributions as in top panel (median ~40mDarcy, maximum ~200mDarcy) and ends with distributions as in bottom panel (median ~2Darcy, maximum ~150Darcy).

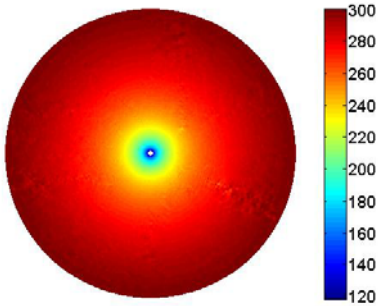

Figure 4: As in Fig 2 for intermediate advective flow rate from outer radius to wellbore; wellbore fluid temperature ~ 120°C.

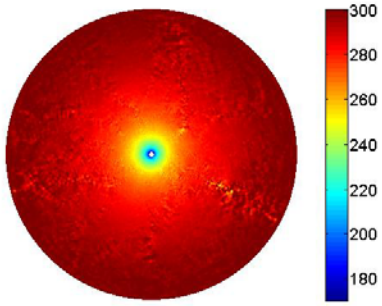

Figure 5: As in Fig 2 for elevated advective flow rate from outer radius to wellbore; wellbore fluid temperature ~ 180°C.

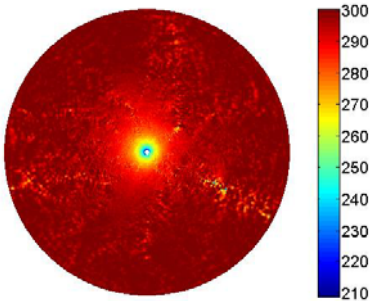

Figure 6: As in Fig 2 for high advective flow rate from outer radius to wellbore; wellbore fluid temperature ~ 210°C.

4. DISCUSSION

Single-wellbore production fluid temperatures of order 200°C indicated by Figs 4-6 for advective flow in 300°C ambient temperature rock offer a significant commercial advantage over the wellbore fluid temperatures of order 80°C constrained by thermal conduction as indicted by Fig 2.

Achieving the controlled flow structure boost illustrated in Figs 4-6 requires, however, demonstration that:

- Wellbore fluid pressurisation can generate sufficient controlled permeability in the rock surrounding the wellbore;
- Achievable stimulation annular radii can provide enough heat over a long enough time period to warrant commercial interest.

The two *in situ* flow sections of Fig 7 illustrate the change in wellbore annular flow regime demanded by the single wellbore heat production boost given by Figs 4-6 for a 10m annular region about the wellbore. In the two flow sections, wellbores at the left edges of the images inject/extract fluid into/out-of the surrounding poroperm medium. The question remains, can the left-hand flow structure be pressure-stimulated (or thermally shocked) into the right-hand flow structure in a controlled manner for commercially relevant volumes?

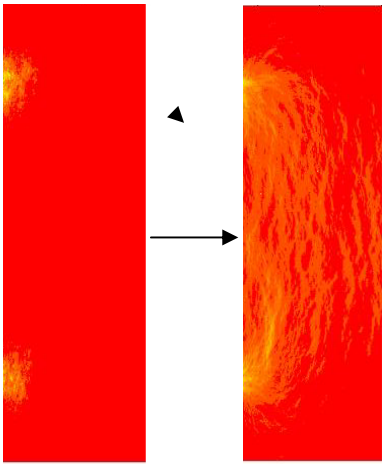

Figure 7: Axial section representation of single wellbore fluid velocity field for un-enhanced permeability field (left) and enhanced permeability field (right). In each panel, fluid from wellbore at left enters into and exits from the geocritical poroperm medium at right. The connecting arrow indicates the permeability enhancement process our *in situ* fluid pressurisation simulation sequence seeks to investigate.

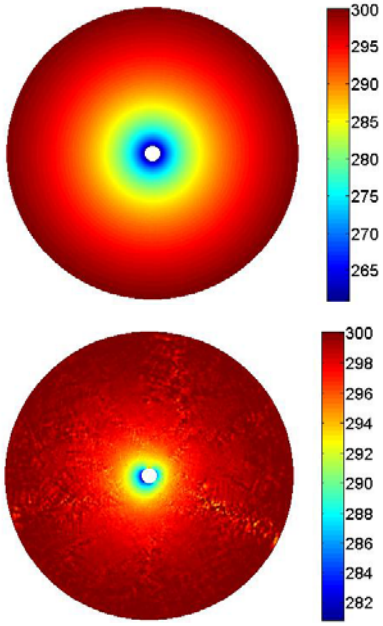

Figure 8: As in Fig 6, except for a 3m outer annular radius and 1kW/m heat extraction rate. (Above/Below) Low/high advective flow; wellbore temperature difference between two rates ~ 20^0C.

Figs 5-6 indicate ~100°C enhancement in wellbore extracted fluid temperature for fluid advection over thermal conductivity in a 10m annulus about a wellbore. It is likely, however, that efforts to exploit a 10m annular radius will proceed through more modest radii. Figs 8-9 estimate the effect of annular heat exchange in a 3m radius by reproducing the comparison between Fig 2 (essentially thermal conductivity) and Figs 4-6 (degrees of fluid advection). Fig 8 shows less than 20°C boost for advection over conduction at the 1kW/m heat extraction rate of Fig 1. If the heat extraction rate is quadrupled as in Fig 9 to correspond to flow in Figs 4-6, the wellbore temperature drops by 100°C but the difference between advection and conduction is if order 30°C.

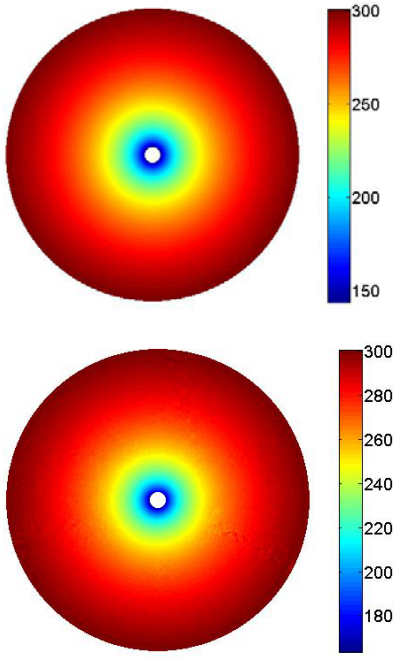

Figure 9: As in Fig 8, except for 4kW/m heat extraction rate. (Above/Below) Low/high advective flow; wellbore temperature ~100°C temperature difference from Fig 8 but temperature difference between low/high advection rates ~ 20^0C

The ~30°C advection/conduction enhancement at 3m radius (Fig 9) and the ~100°C advection/conduction enhancement at 10m radius (Figs 2, 6) suggest that single-well advective heat extraction scales with effective wellbore radius.

The suggested scaling of advective heat extraction with effective radius is at present too dependent on advection modeling assumptions and parameters to be conclusive. To address such matters more effectively we can employ more complex flow simulation code in 3D to simulate field experiments on *in situ* permeability stimulation processes at the modest scale suggested by Figs 8-9 over, say, a 10m section of wellbore in comparison with, say, 10m radius over a 30m section of wellbore. Fig 10 shows a 3-D simulation performed in FEHM (Zyvoloski *et al.* 2011) analogous to the lower simulation permeability distributions of Figs 8-9. Advective and conductive effects are now considered together. The figure represents our access to high performance computational tools capable of simulating complex multi-physics in 3 dimensions. We can, for instance, explore the mechanics of coupled fluid-solid pressure-stress fields interacting with spatially complex

distributions of porosity and permeability (e.g., see appendix).

In parallel with such computations based on in situ permeability enhancement implemented here (see appendix), we can also consider the phenomenon of thermal cracking of hot rock near the wellbore as offering scope for *in situ* investigations of local permeability enhancement. While thermal cracking likely aids the generation of *in situ* permeability, the radial and azimuthal extents at which thermal cracking occurs are not well established (Benson et al 1987; Chun 2013; Grant et al 2013; Tarasovs & Ghassemi 2012). Readily available discussions of *in situ* thermal cracking assume a form of abstract fracture that is not testified to *in situ*. Little or no observational data are cited in relation to attempts to model the thermal fracture process. However, simulations like that of Fig 10 can be used to determine the severe tensile stresses near a wellbore when *in situ* temperatures rapidly decline.

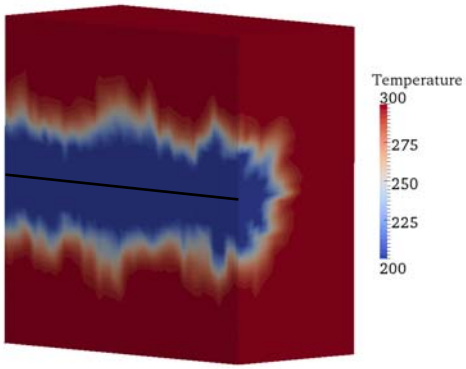

Figure 10: 3-D simulation of temperature field at a horizontal wellbore (black line) in line with 2D simulations of Figs 8-9.

Our working assumption here is that permeability enhancement should be controlled so as to provide reliable flow paths from/to the wellbore. Observations relevant to such an objective are not readily apparent in reports on thermal cracking data. We therefore advance the proposition that even non-commercial scale single-well heat production offers useful access to data on using wellbore-pressurisation of *in situ* fluids to achieve controlled permeability enhancement. The ultimate goal is, of course, to gain insight into practical means by which *in situ* fluid pressurisation might accomplish commercial scales of wellbore-to-wellbore flow in hot crustal rock.

5. CONCLUSIONS

Heat advection simulations for media over a range of permeability distributions and median values indicate that advective systems can substantially out-produce conduction-limited single-well heat extraction installations. Given the large number of presently unused single-well flow systems in geothermal fields, some may prove to have a form of commercial viability. Further, as almost all the *in situ* issues pertaining to geothermal energy extraction are encapsulated in the mechanics of flow systems that can in principle be realised in a single-well context, we suggest that single-well flow systems can be used cost-effectively to study the *in situ* mechanics of permeability enhancement. Many geothermal fields have large numbers of non-producing wells that could be used as appropriate-scale *in situ* laboratories for studying *in situ* permeability enhancement with temperature as a primary observable with which to measure the radial and axial spatial extent and degree of increased permeability.

REFERENCES

Benson SM, Daggett JS, Iglesias E, Arellano V & Ortiz-Ramirez J (1987) Analysis of thermally induced permeability enhancement in geothermal injection wells, *Proceedings 12th Workshop on Geothermal Reservoir Engineering*, Stanford University, Stanford, California, January 20-22, 1987.

Carslaw HS & Jaeger JC (1959) *Conduction of Heat in Solids*, Clarendon Press, Oxford, pp510.

Chun K (2013) Fracture propagation under poro-thermally induced stress using the displacement discontinuity method, *Proceedings 38th Workshop on Geothermal Reservoir Engineering*, Stanford University, Stanford, California, February 11-13, 2013

Freeze RA (1975), A Stochastic-Conceptual Analysis of One-dimensional Groundwater Flow in Non-uniform Homogeneous Media, *Water Resources Research*, 11, 725-741.

Grant MA, Clearwater J, Quinão, J, Bixley PF & Le Brun M (2013) Thermal stimulation of geothermal wells: a review of field data, *Proceedings 38th Workshop on Geothermal Reservoir Engineering*, Stanford University, Stanford, California, February 11-13, 2013

Gringarten AC & Witherspoon PA (1973) Extraction of Heat from Multiple-Fractured Dry Hot Rock, , Geothermics, V.2 No. 3-4, 119-122

Hanano M (2000) Two different roles of fractures in geothermal development, *Proceedings World Geothermal Congress 2000*, Kyushu - Tohoku, Japan, May28-June10.

Horne RN & Rodriguez FJ (1985) Dispersion in tracer flow in fractured geothermal Systems, *Proceedings 7th Workshop on Geothermal Reservoir Engineering*, Stanford University, Stanford, CA

Ito T & Hayashi K (2003) Role of stress-controlled flow pathways in HDR geothermal reservoirs, *Pure appl. Geophys.* 160, 1103–1124.

Jensen, JL, Hinkley DV, & Lake LW (1987) A statistical study of reservoir permeability: distributions, correlations, and averages: SPE Formation Evaluation, December 1987

Juliusson E (2012) Characterization of fractured geothermal reservoirs based on production data, Stanford Geothermal Program, Stanford University, Stanford, CA

Kittridge MG, Lake LW, Lucia FJ & Fogg GE (1990) Outcrop/Subsurface Comparisons of Heterogeneity in the San Andres Formation, *SPE Formation Evaluation*, September, 233-240

Kwon KC (1998) Heat transfer model of above and underground insulated piping systems, WSRC-MS-98-0038, ASME Conference – Heat Exchanger Committee & Joint Power Generation Conference, Baltimore MD.

Law J (1944) A statistical approach to the interstitial heterogeneity of sand reservoirs: Technical Publication 1732, Petroleum Technology v. 7, May 1944.

Leary P, Pogacnik J & Malin P (2012) An empirical basis for EGS flow stimulation mechanics, *Proceedings New Zealand Geothermal Workshop*, Auckland, 17-19 Nov 2012.

Leary P, Pogacnik J & Malin P (2012) Fractures ~ Porosity --> Connectivity ~ Permeability --> EGS Flow Stimulation, *Proceedings Geothermal Resources Council 36th Annual Conference*, 30 Sep – 3 Oct, Reno NV.

Leary P, Pogacnik J & Malin P (2012) Computational EGS -- Heat transport in 1/*f*-noise fractured media, *Proceedings 37th Stanford Geothermal Workshop*, 30Jan-1Feb, Stanford University.

Leary, PC (2002) Fractures and physical heterogeneity in crustal rock, in *Heterogeneity of the Crust and Upper Mantle – Nature, Scaling and Seismic Properties,* J. A. Goff, & K. Holliger (eds.), Kluwer Academic/Plenum Publishers, NewYork, 155-186.

Leary PC & Al-Kindy F (2002) Power-law scaling of spatially correlated porosity and log(permeability) sequences from north-central North Sea Brae oilfield well core, *Geophysical Journal International* **148**, 426-442.

Limpert E, Stahel W & Abbt M (2001) Log-normal Distributions across the Sciences: Keys and Clues, *BioScience*, v.51, no. 5, 341–352.

Pogacnik J, Leary P & Malin P (2012) Physical/computational framework for EGS *in situ* fracture stimulation, *Proceedings New Zealand Geothermal Workshop*, Auckland, 17-19 Nov 2012.

Pogacnik J, Leary P & Malin P (2013) CGS – Controlled wellbore-to-wellbore geothermal system flow, *Proceedings 38th Stanford Geothermal Workshop*, 11-13 Feb, Stanford University.

Pruess K & Narasimhan TN (1985) A practical method for modeling fluid and heat flow in fractured porous media, *Society of Petroleum Engineers Journal*, SPE10509, 14-26.

Ramey, HJ (1962) Wellbore heat transmission, 36th Society of Petroleum Engineers Annual Meeting, Dallas TX, 8-11 October, SPE 96.

Sandve TH, Berre I, Keilegavlen E & Nordbotten JM (2013) Multiscale simulation of flow and heat transport in fractured geothermal reservoirs: inexact solvers and improved transport upscaling , Proceedings 38th Workshop Geothermal Reservoir Engineering, Stanford University, Stanford CA, February 11-13.

Sutter D, Fox DB, Anderson BJ, Koch DL, von Rohr PR &Tester JW (2011) Sustainable heat farming of geothermal systems: a case study of heat extraction and thermal recovery in a model EGS fractured reservoir, *Proceedings 36th Workshop on Geothermal Reservoir Engineering*, Stanford University, January 31-February 2.

Tarasovs S & Ghassemi A (2012) On the role of thermal stress in reservoir stimulation, *Proceedings 37th Workshop on Geothermal Reservoir Engineering*, Stanford University, Stanford, California, January 30 - February 1, 2012

Taylor DW (1948). *Fundamentals of Soil Mechanics*, John Wiley & Sons, NY.

Tester JW et al (2006) The Future of Geothermal Energy, http://geothermal.inel.gov; http://www1.eere.energy.gov/geothermal/egs_technology.html

US Energy Information Administration, 2011, Distribution and Production of Oil and Gas Wells by State: http://www.eia.gov/;

Warren JE & Skiba FF, 1964, Macroscopic dispersion, Society of Petroleum Engineers Journal, SPE648, 215-230.

Watanabe K & Takahashi H (1995) Fractal geometry characterization of geothermal reservoir fracture networks *Journal Geophysical Research* 100, B1, 521-528.

Zyvoloski G, Robinson B, Dash Z, Kelkar S, Viswanathan H, Pawar R, & Stauffer P (2011). "Software Users Manual for the FEHM Application Version 3.1.0." Los Alamos National Laboratory, LA-UR-12-24493.

APPENDIX – NOTES ON PERMEABILITY ENHANCEMENT VIA *IN SITU* FLUID PRESSURISATION

In situ fractures have long been understood to be a primary means of fluid flow in geothermal reservoirs (e.g., Gringarten &Witherspoon 1973; Pruess & Narasimhan 1985; Horne & Rodriguez 1985; Watanabe & Takahashi 1995); Hanano 2000; Ito & Hayashi 2003; Tester et al 2006; Sutter 2011; Juliusson 2012; Sandve et al 2013). For the most part in such discussions fractures figure in reservoir flow concepts as discrete quasi-planar geometric discontinuities in an otherwise quasi-uniform porous medium, with fracture assemblages given by normally-distributed statistically-independent fracture parameters (e.g., length, position, strike, dip, width).

By the central limit theorem, collections of normally-distributed statistically-independent events tend to retain a collective normal distribution (Limpert, Stahel & Abbt 2001). Such fracture-flow concepts are inconsistent with observed lognormality of geothermal well productivity (e.g., Grant 2009). Available evidence suggests that geothermal reservoir flow processes do not differ greatly from flow processes in other crustal volumes (Leary et al 2013b). With respect to understanding prospects for increased heat extraction in single geothermal wells, it may be cogently observed that lognormality of crustal flow systems is the rule rather than the expectation: oil/gas field reservoir well-core permeability is lognormally distributed (Law 1944; Warren & Skiba 1964; Freeze 1975; Kittridge et al 1990; Leary & Al Kindy 2002), as are oil/gas well productivities (USEIA 2011) and ore-grades and trace-element abundances (Leary, Pogacnik & Malin 2012b).

Lognormal distributions of *in situ* permeability and flow systems are intrinsically consistent with well-log and well-core empirics that comprise the 'geocriticality' aspect of crustal fluid flow. As discussed by Leary et al (2012a,b), geocriticality treats flow via *in situ* fractures as percolation along spatially-correlated grain-scale cement-bond defect pathways that are fully integral to the rock fabric rather than as flow through geometric discontinuities in the rock fabric. The key difference in the two views of *in situ* fractures is that geocriticality is defined by a specific well-log fluctuation spectrum ($S(k) \sim 1/k^1$) that is inherently spatially-correlated and is almost everywhere observed in crustal rock, while fracture systems defined by normally-distributed statistically-independent geometric discontinuities have a (notional) well-log spectrum ($S(k) \sim 1/k^0 \sim const$) and that is rarely if ever observed *in situ*.

Geocriticality affords an empirical basis for enhancing *in situ* permeability through its poroperm relation $\kappa \sim \exp(\alpha\varphi)$ (e.g., Leary et al (2012a,b); a similar relation exists for clays (Taylor 1948). Figs A1-A2 illustrate the *in situ* relation $\kappa \sim \exp(\alpha\varphi)$ for two sets of clastic reservoir well-core data. In each subplot, blue dots trace well-core logκ as a function of well-core φ. Above each plot is the value of the parameter α determined by the red-line fits to the data trends.

The empirical α values in Figs A1-A2 cluster around 16 for the North Sea reservoir and 28 for the South Australia tight gas sands, with low values ~10 for both data sets. Fig 3 above shows how these α values translate into degrees of lognormality associated with each of these values, with increasing α giving higher permeability and higher advective heat transport as shown by the Fig 4-6 temperature distributions. Figs A1-A2, and 3-6 thus encapsulate the empirics of *in situ* permeability distributions associated with geocriticality.

The geomechanics of *in situ* percolation flow through spatially-correlated grain-scale fracture density fluctuations is pictured in Fig A3 for radial fluid flow in a wellbore-centered annulus at set up in the Matlab PDE solver. The contours in the annulus indicate spatial trajectories by which *in situ* fluids percolate from the wellbore to the outer annular radius via grain-scale fracture-connectivity pathways determined by the porosity structure of the poroperm medium and by the value of lognormality parameter α. The sidebar indicates that many fracture-connectivity pathways conduct fluid at 10 to 20 times the rate of much of the annulus.

These flow simulations suggest that permeability stimulation can proceed through *in situ* fluid pressurisation, but it is likely that fluid-solid interaction is strongly coupled to the existing porosity distribution within the stimulation volume.

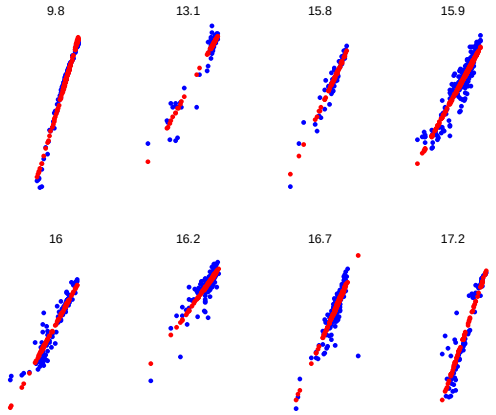

Figure A1: Poroperm cross-plots for eight North Sea reservoir well-core data sequences. For each poroperm sequence porosity is plotted along the x-axis and logarithm of permeability is plotted along the y-axis. The mean plot trend for each sequence is given by the red line; the line slope above each plot is the value of the α-parameter in lognormality relation $\kappa \sim exp(\alpha\varphi)$.

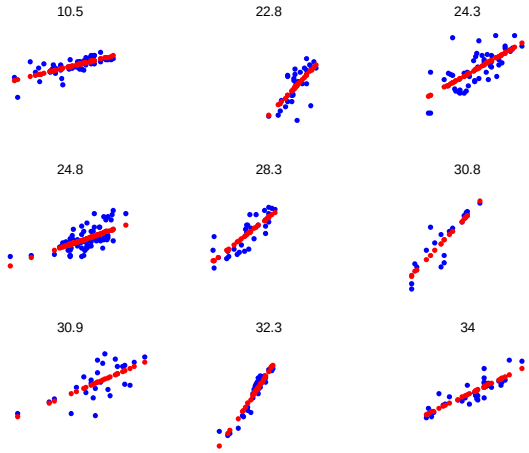

Figure A2: Poroperm data sequences as in Fig A1, for well-core from tight gas formations in South Australia

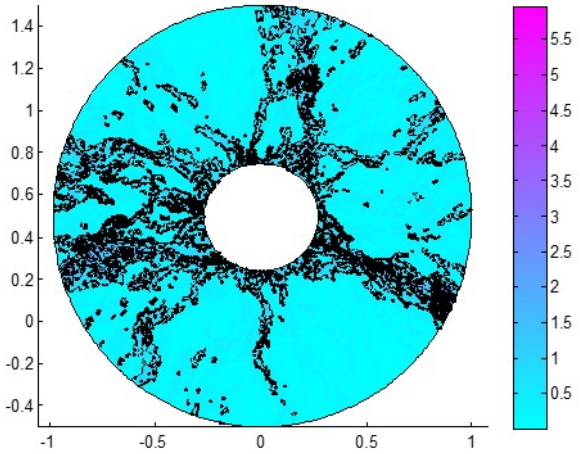

Figure A3: Fluid-flow velocity distribution in annular section of geocritical poroperm medium. Permeability distribution of the medium related to porosity distribution as $\kappa \sim exp(\alpha\varphi)$. Fluid velocity given by Darcy flow, $v(x,y) = \kappa(x,y)\nabla P(x,y)$, for pressure/flow boundary conditions at inner/outer radii. Numerical solution by Matlab PDE solver.